Dalton Transactions

RSC Publishing

PAPER

View Article Online
View Journal | View Issue

Cite this: *Dalton Trans.*, 2013, **42**, 12688

Synthesis and characterization of conjugated Dawson-type polyoxometalate–porphyrin copolymers†

Iban Azcarate,[a,b,c] Iftikhar Ahmed,[d] Rana Farha,[e,f] Michel Goldmann,[e,g] Xiaoxia Wang,[h] Hualong Xu,[h] Bernold Hasenknopf,*[a] Emmanuel Lacôte*[b,i] and Laurent Ruhlmann*[c,d]

Received 29th March 2013,
Accepted 30th April 2013

DOI: 10.1039/c3dt50850a

www.rsc.org/dalton

Hybrid polyoxometalate–porphyrin copolymeric films were obtained by the electro-oxidation of zinc octaethylporphyrin (ZnOEP) in the presence of a Dawson type polyoxophosphovanadotungstate bearing two pyridyl groups (POM(py)$_2$). The synthesis of a series of POM(py)$_2$ consisting of $[P_2W_{15}V_3O_{62}]^{9-}$ functionalized with diol-amide or triol moieties, as well as the characterization of the copolymers are presented.

Introduction

Polyoxometalates (POMs) are a structurally diverse family of anionic metal oxide molecular compounds with applications in analytics, medicine, catalysis and photocatalysis, electronics and materials science.[1] One of the most interesting features of POMs is their rich photoredox chemistry.[2] Typically, upon light irradiation electrons are promoted from an oxygen-centered 2p orbital to an empty metallic d-orbital, generating a highly reactive charge-separated state. The photoexcited POM has an increased oxidizing power, and organic substrates can be oxidized while the POM is converted into its reduced form. The latter can subsequently be re-oxidized with molecular oxygen or by reducing a second substrate.

Interestingly, owing to their robustness and large number of metallic centers, POMs can undergo reversible and multi-electron photoredox processes without decomposition. However, in most of the cases, the O → M ligand-to-metal charge transfer (LMCT) absorption band lies in the UV region (λ = 200–400 nm) which strongly limits the use of POMs in solar visible light conversion materials.

In order to overcome this problem, POMs can be linked to visible light sensitive molecules *via* covalent, coordination or non-covalent bonding.

The non-covalent approach is based on van der Waals or Coulombic interactions and does not need POM pre-functionalization. Since POMs are anionic clusters, they can form electrostatic complexes with cationic chromophores such as Ru or Re polypyridyl complexes,[3–5] organic dyes,[6–8] or porphyrins and phthalocyanines.[9–11]

POM–porphyrin coordination complexes were also reported.[12–15] However, stronger POM–chromophore bonds are required to avoid dissociation and ensure better electronic communication.

The third approach is based on covalent linkage between the POM and the visible light photosensitizer. The recent progress in organo-polyoxometalate chemistry ensures that virtually any organic function can be added to POM structures, whose design can be synthetically controlled.[16,17]

The use of a spacer adds versatility. Hence, functional molecular devices with varied POM/chromophore ratios, spatial geometry, *etc.* can be obtained.

Several covalent donor–acceptor dyads based on POMs were prepared using ferrocenyl,[18,19] pyrene and perylene,[20–22] Ru and Ir complexes,[21,23] and porphyrins.[24–27]

The introduction of POM–chromophore hybrids into polymeric and surface supported materials is the next step toward functional devices with catalytic, optic or photovoltaic properties.[28]

[a]*UPMC Univ Paris 6, Institut Parisien de Chimie Moléculaire, CNRS UMR 7201, 4 Place Jussieu, 75005 Paris, France. E-mail: bernold.hasenknopf@upmc.fr*
[b]*ICSN CNRS, Av. de la Terrasse, 91198 Gif-sur-Yvette Cedex, France*
[c]*Université de Strasbourg, Laboratoire d'Electrochimie et de Chimie Physique du Corps Solide, Institut de Chimie, 4 rue Blaise Pascal CS 90032, F-67081 Strasbourg Cedex, France. E-mail: lruhlmann@unistra.fr*
[d]*Université Paris-Sud 11, Laboratoire de Chimie Physique, U.M.R. 8000 CNRS, Bâtiment 349, 91405 Orsay cedex, France*
[e]*UPMC Univ Paris 6, Institut des NanoSciences de Paris, CNRS UMR 7588, 4 place Jussieu, 75005 Paris, France*
[f]*Laboratoire d'Analyse et Contrôle des Systèmes Complexes - LACSC-ECE Paris Ecole d'Ingénieurs, 37 Quai de Grenelle, F - 75015 Paris, France*
[g]*Université Paris Descartes, 45 rue des Saints Pères, F - 75006 Paris, France*
[h]*Department of Chemistry, Shanghai Key Laboratory of Molecular Catalysis and Innovative Materials and Laboratory of Advanced Materials, Fudan University, Shanghai 200433, People's Republic of China*
[i]*Université de Lyon, Institut de chimie de Lyon, UMR 5265 CNRS-Université Lyon I-ESCPE Lyon, 43 Bd du 11 novembre 1918, 69616 Villeurbanne, France. E-mail: emmanuel.lacote@univ-lyon1.fr*

†Electronic supplementary information (ESI) available. See DOI: 10.1039/c3dt50850a

The alternate deposition of anionic POMs and cationic sensitizers such as metal complexes,[29,30] organic dyes[31,32] and porphyrins[33,34] on surfaces using the layer-by-layer (LbL) technique generates thin-films with controlled thickness. Some of us recently reported the first POM cationic porphyrin-based photovoltaic multilayered film obtained by LbL showing photocurrent production under visible-light irradiation.[34]

Peng reported the synthesis of an Fe(terpyridine)$_2$-Lindqvist molybdate coordination polymer[35] as well as hybrid (co)polymers with conjugated photoactive backbones and the POM inserted in the main-chain[36,37] or as a side-chain pendant.[38,39] A photovoltaic device constructed from the POM main-chain containing polymer showed a power conversion of 0.15%.[37] More recently, we reported the formation of a mixed POM–porphyrin copolymer film with an Anderson type POM $[MnMo_6O_{18}\{(OCH_2)_3CNHCO(4\text{-}C_5H_4N)\}_2]^{3-}$ and ZnOEP *via* an original electropolymerization/deposition process. The photoactive film was used as a heterogeneous photocatalyst for the reduction of Ag^+ under visible light.[40]

However, none of the polymers examined thus far were based on POMs with reversible redox behavior, and conjugated spacers. In the present paper, we introduce such covalently bonded conjugated POM–porphyrin copolymers using our $[P_2W_{15}V_3O_{62}]^{9-}$ diolamide-grafting method[41] toward devising more efficient photoactive films. We report herein the bottom-up synthesis and characterization of films obtained from bis-pyridine-substituted molecular organo-polyoxometallic bricks with different geometries, and examine the influence of the monomer structure on the architecture of the polymers as a prerequisite to understand their photocatalytic properties.

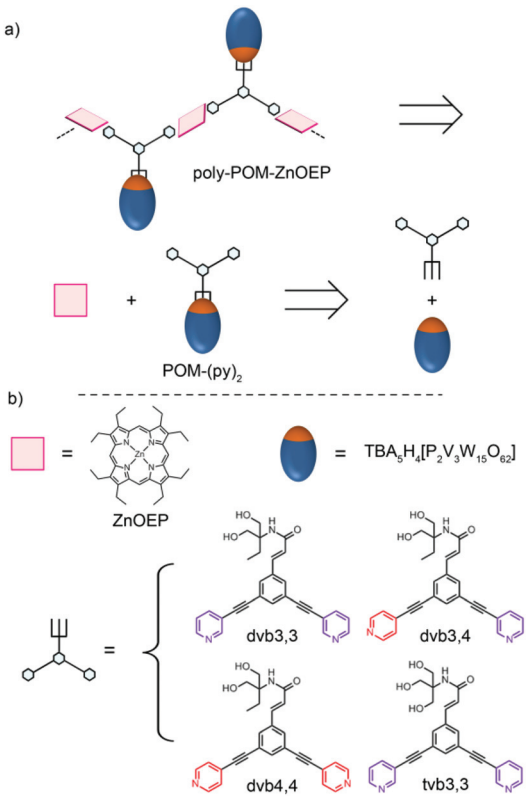

Scheme 1 (a) Schematic representation of the two step synthesis of a POM–porphyrin copolymer using molecular building blocks. (b) Representation of ZnOEP, $TBA_5H_4[P_2V_3W_{15}O_{62}]$ and the tris- (**tvb3,3**) or diol-amide (**dvb3,3**, **dvb3,4** and **dvb4,4**) ligands.

Results and discussion

Our strategy for the synthesis of the films relies on the electrocopolymerization of porphyrins with several bis-pyridine-capped phosphovanadotungstates $[P_2W_{15}V_3O_{62}]^{9-}$ (Scheme 1). The organo-POM monomer was designed around 1,3,5-trisubstituted benzene rings, which serve as conjugated turntables. Two of the substituents were connected to the pyridines (two needed for polymerization), while the last one was connected to the POM. We used one porphyrin (zinc octaethylporphyrin, ZnOEP), and selected four organic connectors. Three of them relied on the diolamide coupling[41] to establish full conjugation in the polymer between the organic backbone and the pendant POM framework through the incorporated carbonyl function. They differed by the relative positions of the two nitrogen atoms of the pyridines (3,3; 3,4; 4,4), while the fourth was a triol-capping ligand,[42] chosen to assess the exact role of the conjugation to the POM.

Preparation of the organic ligands

The preparation of the diolamine/triolamine bis-pyridine ligands started with 1,3,5-tribromobenzene (**1**, Scheme 2), which was carbonylated to 3,5-dibromobenzaldehyde (**2**) *via* its mono-lithiated anion.[43] The aldehyde was olefinated to ester **3** *via* a Wittig reaction.[44] **3** was a key intermediate to the four ligands of this study, which were obtained *via* double Pd-catalyzed Sonogashira cross-coupling. **3** was doubly coupled to 3-ethynylpyridine in the presence of tetrakis(triphenylphosphine) palladium, CuI and triethylamine,[45] quantitatively leading to **evb3,3**.

However, the same reaction from 4-ethynylpyridine hydrochloride only gave the mono-coupled product in poor yield. We changed the solvent system to DMF–Et_3N (2 : 1) and it was then possible to isolate the bisethynylpyridine derivative (**evb4,4**, 55%) together with some remaining mono-coupled **evb4,Br** (26%), which were separated by column chromatography. Interestingly, the isolation of the latter allowed us to prepare the dissymmetric cinnamic ester **evb3,4** *via* a Sonogashira coupling with 3-ethynylpyridine (65%). The diol and triol functions were then installed *via* amide formation from 2-amino-2-ethyl-1,3-propanediol and 2-amino-2-(hydroxymethyl)-1,3-propanediol, as reported previously.[41,42] The former delivered ligands **dvb3,3** (for diolamide vinyl benzoate ethynyl 3-pyridine, ethynyl 3-pyridine), **dvb3,4** and **dvb4,4** in 80%, 75% and 60% yields respectively. The latter gave **tvb3,3** (for triolamide vinyl benzoate ethynyl 3-pyridine, ethynyl 3-pyridine) in 60% yield.

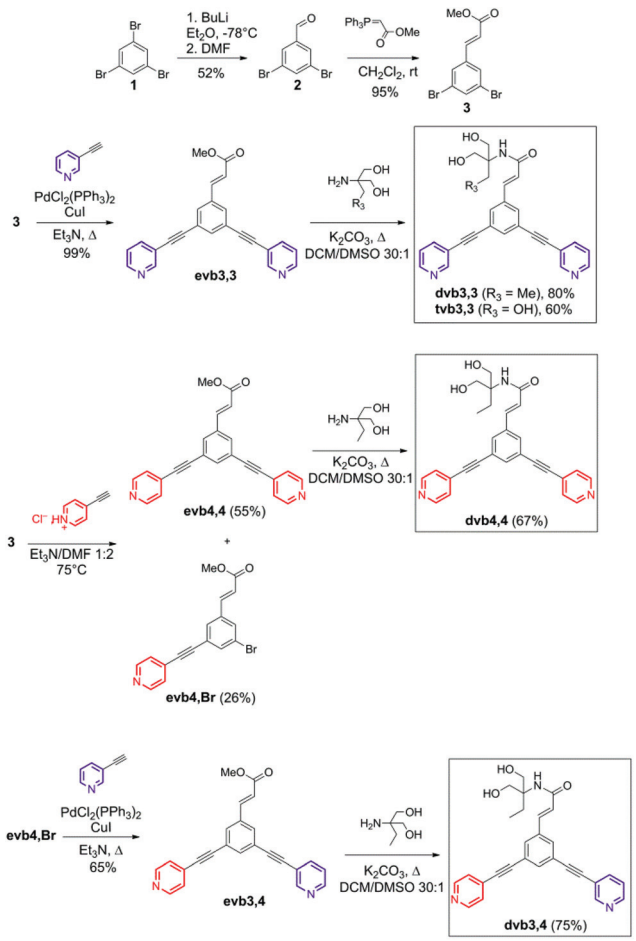

Scheme 2 Synthesis of the ligands **dvb3,3**, **dvb3,4**, **dvb4,4** and **tvb3,3**.

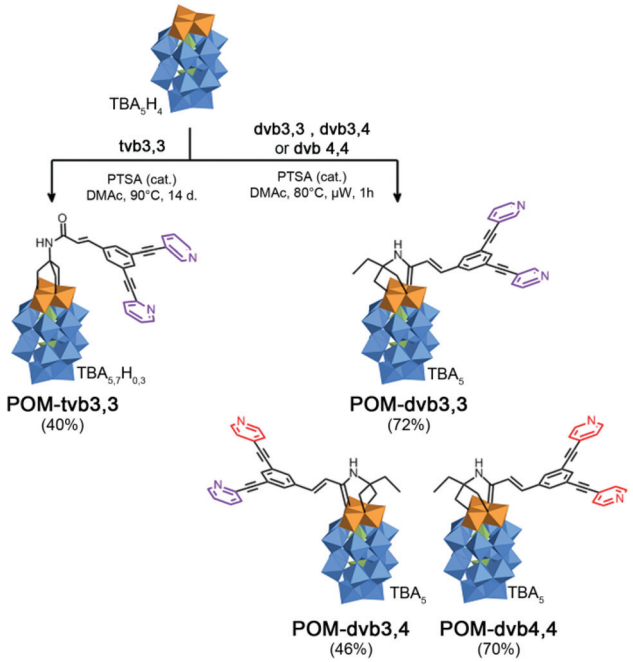

Scheme 3 Synthesis of **POM-tvb3,3**, **POM-dvb3,3**, **POM-dvb3,4** and **POM-dvb4,4**.

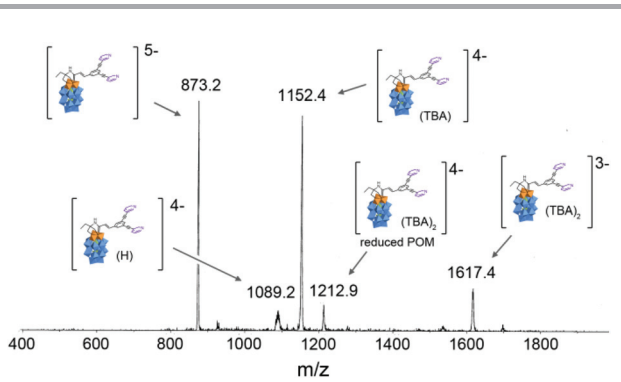

Fig. 1 Obtained ESI MS data for **POM-dvb3,3** solution in CH_3CN (50 μM).

Preparation of the organo-POM monomers

$TBA_5H_4[P_2V_3W_{15}O_{62}]$ was reacted with the diol-amide ligands **dvb3,3**, **dvb3,4** and **dvb4,4** in DMAc at 80 °C under microwave irradiation (Scheme 3, right).[41] The desired organic–inorganic POM hybrids **POM-dvb3,3**, **POM-dvb3,4** and **POM-dvb4,4** were isolated in 72%, 46% and 70% yields, respectively after several purifications by selective precipitation with ethanol or ether from an acetonitrile solution. Triol **tvb3,3** was converted to **POM-tvb3,3** upon heating it at 90 °C in the presence of $TBA_5H_4[P_2V_3W_{15}O_{62}]$ for 2 weeks (50% yield).[42] The four organo-POM monomers were fully characterized by ^1H, ^{13}C and ^{31}P NMR, MS, IR, UV-Vis spectroscopy, elemental analysis and electrochemistry.

Characterizations of the organo-POM monomers

IR characterization. The IR spectra of the hybrid monomers showed peaks at 1087 (ν_{P-O}), 950 ($\nu_{W=O}$), 900 (ν_{W-Oc-W}), 815 (ν_{W-Oe-W}) cm^{-1}, which are characteristic of the Dawson phosphovanadotungstate.[46,47] The signals corresponding to the organic part were found at the expected wavenumbers, albeit weak due to the relatively low content in the hybrids.

Mass spectrometry. Fig. 1 presents an ESI-MS spectrum obtained for the **POM-dvb3,3** hybrid. The main peak corresponds to the 5-ion stripped of all cations. Peaks assignable to the clusters associated with one TBA, one H^+ or two TBA cations were also observed. Also, the reduced form of the hybrid – most likely produced during the ionization process – was detected (minor peaks). The other POM monomers behaved similarly (see ESI†).

NMR characterization. The ^{31}P NMR of all hybrids reveals only two signals around −7 and −13 ppm. This confirms the presence of the two chemically inequivalent phosphate templates of the Dawson structure, and proves that the hybrid is free of unfunctionalized $[P_2W_{15}V_3O_{62}]^{9-}$, or any P-containing degradation product. The ^1H NMR spectra present the signals from the grafted organic bipyridyl ligands (around 7 ppm), the diols (or triol) and the TBA counterions.

The chemical shift differences between the functionalized and the free organic part ($\Delta\delta$, in ppm) are reported in Table 1. The full comparison of the chemical shifts of the free ligand

Table 1 ^{1}H NMR chemical shift difference ($\Delta\delta$ in ppm) between the POM(py)$_2$ hybrid and the free ligand

		POM-dvb3,3	POM-dvb3,4		POM-dvb4,4	POM-tvb3,3
CH_2OV		1.81	1.94		1.72	2.02
Ethylenic	$H_{Et}(1)$	1.22	1.21		0.83	−0.02
	$H_{Et}(2)$	0.63	0.54		0.41	0.04
Aromatic	$H_{Ar}(1)$	0.71	0.92/0.67		0.67	0.07
	$H_{Ar}(2)$	0.19	0.20		0.11	0.04
			3py	4py		
Pyridine	H^2	0.06	0.12	0.23	0.24	0.04
	H^3	—	—	0.18	0.14	—
	H^4	0.06	0.10	—	—	0.07
	H^5	0.24	0.23	0.18	0.14	0.07
	H^6	0.33	0.31	0.23	0.24	0.07

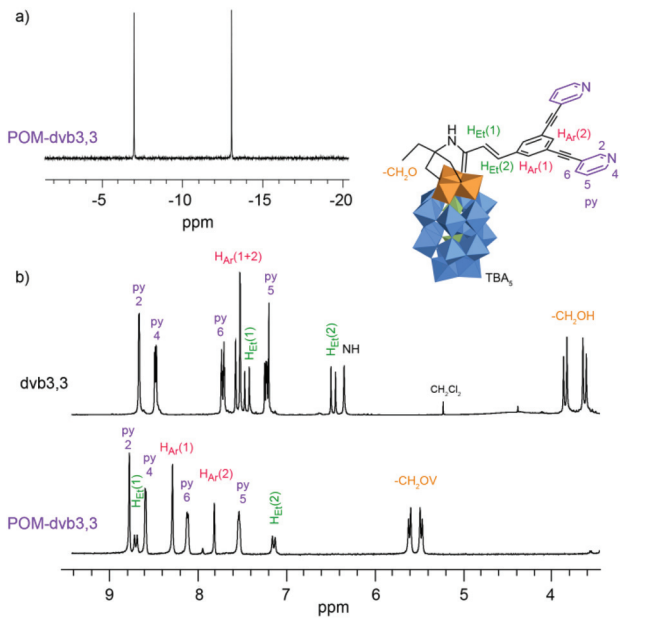

Fig. 2 (a) ^{31}P NMR spectrum of **POM-dvb3,3** in CD_3CN. (b) ^{1}H NMR spectra of **dvb3,3** in $CDCl_3$ and **POM-dvb3,3** in CD_3CN, zoom of the aromatic region.

and those of the grafted ones (Fig. 2b for **POM-dvb3,3**) gave strong evidence of the covalent grafting of the organic part. In particular, the signal for the CH_2OH is strongly deshielded (about 1.8 ppm) upon attachment to the vanadate cap. This is likely caused by the strong electron withdrawing effect of the POM. Interestingly, the presence of the POM impacts all the signals of the organic part in the diol-amide chemistry but only small chemical shift changes were observed in the case of triol functionalized hybrids ($\Delta\delta_{max}$ = 0.07 ppm, except for CH_2OV). We believe this is a further indication that the carbonyl incorporation into the POM structure induces a good electronic communication between the inorganic and the organic parts (effect over more than ten C–C bonds), while in the case of triol functionalization, the electronic effects of the POM are limited to the first C–C bond.

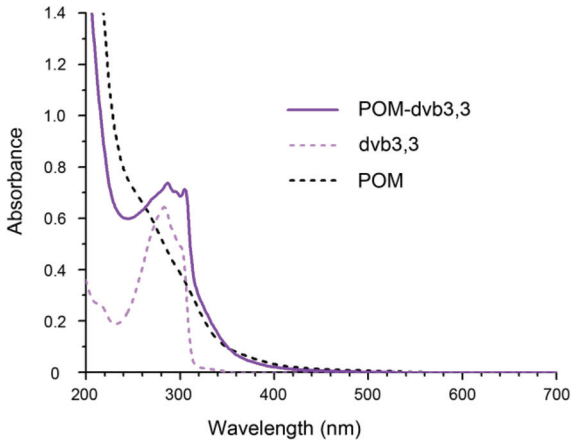

Fig. 3 UV-vis absorption spectra of **POM** (black dotted curve), **dvb3,3** (light dotted purple curve) and **POM-dvb3,3** (plain purple curve) in CH_3CN solution (c = 6.25 × 10^{-6} M). POM = $[P_2V_3W_{15}O_{62}]^{9-}$.

UV-visible characterization. The UV spectra of the hybrids are the sum of the oxygen-to-metal charge transfer (LMCT) bands and the organic ligand absorbance around 280 nm (Fig. 3). The combined bands extend to the visible, which explains the yellow color of the POM(py)$_2$ hybrids.

Cyclic voltammetry and differential pulse voltammetry. The cyclic voltammograms and differential pulse voltammograms of **POM-tvb3,3**, **POM-dvb4,4**, **POM-dvb3,4**, **POM-dvb3,3** and the parent POM $[P_2V_3W_{15}O_{62}]^{9-}$ show three monoelectronic successive reductions, corresponding to the reversible reduction of the three V^V between +0.1 V and −0.9 V *vs.* SCE. It is the first time that separate waves for the reduction of the three V^V are observed. Indeed, only two reversible redox processes concerning V^V were reported by Hill[42] for $[P_2V_3W_{15}O_{62}]^{9-}$ and triol-capped $[CH_3C(CH_2O)_3P_2V_3W_{15}O_{59}]^{6-}$. Similarly, we have observed that in the porphyrin/triol-capped $[P_2V^V{}_3W_{15}O_{59}$-{$(OCH_2)_3C$–NHC(=O)(ZnTPP)}],[27] the first reduction process of the trivanadium cap involves one electron, while the second process involves the two other V^V atoms together.

In the present study, $[P_2V^V{}_3W_{15}O_{62}]^{9-}$ shows two successive reduction processes. However, its differential pulse voltammogram presents a tiny splitting of the second process, suggesting that two close monoelectronic waves are present (bottom of Fig. 4). In the case of **POM-tvb3,3**, **POM-dvb4,4**, **POM-dvb3,4** and **POM-dvb3,3**, the splitting of the second process is well observed. The reduction potential of the trivanadate cap depends mostly on the type of grafting (compare curves in Fig. 4 with **tvb** and **dvb** grafting), as one would expect for such structures (Table 2).

Finally, the difference between the oxidative and the reductive peak potentials (ΔE_p) increases after each reduction of the V^V. For example, ΔE_p for the first, second and third reductions of V^V measured for **POM-tvb3,3** are 104, 220, and 325 mV respectively (Table 2). This indicates that the electron transfer becomes increasingly slow, in agreement with the localization of the added electrons in the vanadium cap, where

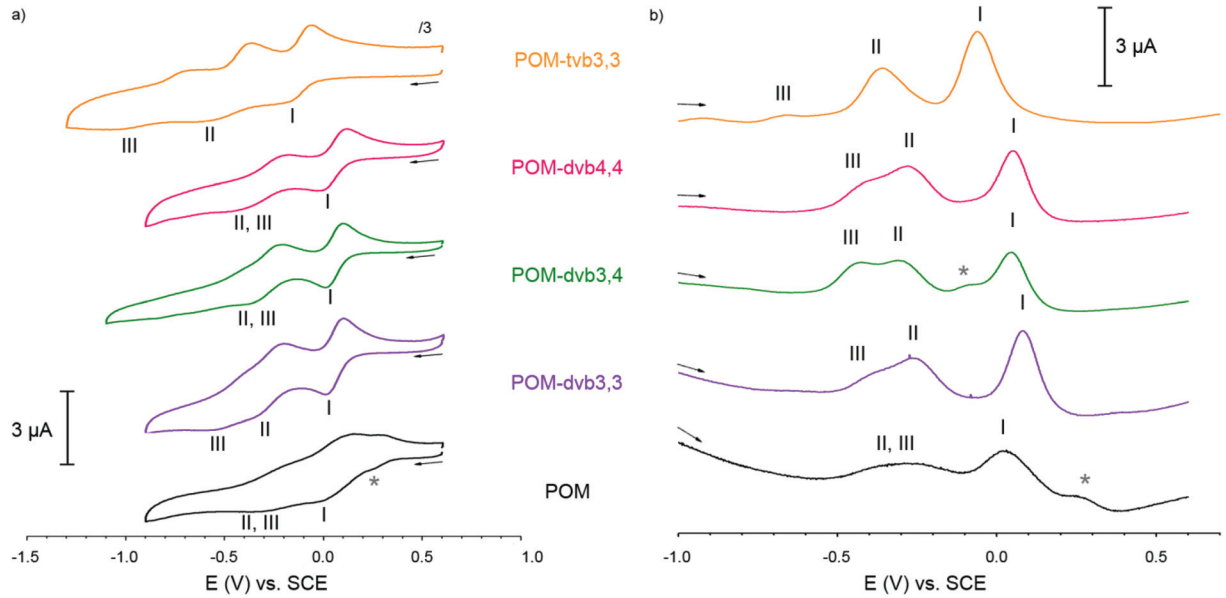

Fig. 4 (a) Cyclic voltammograms of **POM-tvb3,3**, **POM-dvb4,4**, **POM-dvb3,4**, **POM-dvb3,3**, and $TBA_5H_4[P_2V_3W_{15}O_{62}]$ at $c = 5 \times 10^{-4}$ mol L^{-1} and $v = 10$ mV s^{-1}. (b) Differential pulse voltammograms at 25 mV s^{-1} in 1,2-$C_2H_4Cl_2$–CH_3CN (7/3), containing 0.1 mol L^{-1} NBu_4PF_6. Working electrode: glassy carbon. *Adsorption peak.

Table 2 Electrochemical data for **POM-tvb3,3**, **POM-dvb3,3**, **POM-dvb3,4** and **POM-dvb4,4** and copolymers **poly-POM-tvb3,3-ZnOEP**, **poly-POM-dvb3,3-ZnOEP**, **poly-POM-dvb3,4-ZnOEP** and **poly-POM-dvb4,4-ZnOEP**[a]

	Oxidation	Reduction				
	π-Ring	V^V/V^{IV}			py+	π-Ring
POM-tvb3,3		−0.11[b] (104)	−0.48[b] (220)	−0.85[b] (325)		
POM-dvb3,3		0.06[b] (87)	−0.26[b] (117)	−0.43[b] (166)		
POM-dvb3,4		0.06[b] (84)	−0.29[b] (139)	−0.43[b,e]		
POM-dvb4,4		0.06[b] (113)	−0.31[b] (222)	−0.41[b,e]		
ZnOEP	0.94/0.68					−1.60[b]
poly-POM-tvb3,3-ZnOEP					−1.02[irr,c]	−1.70[c]
poly-POM-dvb3,3-ZnOEP		[d]	[d]	[d]	−1.02[irr,c]	−1.32[irr,c]
poly-POM-dvb3,4-ZnOEP		[d]	[d]	[d]	−0.87[irr,c]	−1.47[irr,c]
poly-POM-dvb4,4-ZnOEP		[d]	[d]	[d]	−0.79[irr,c]	−1.54[irr,c]

[a] All potentials in V *versus* SCE were obtained from cyclic voltammetry in 1,2-$C_2H_4Cl_2$–CH_3CN (7 : 3) containing 0.1 mol L^{-1} $(NBu_4)PF_6$. Scan rate = 0.1 V s^{-1}. [b] Working electrode: glassy carbon electrode. [c] ITO, $S = 1$ cm^2 after 25 scans. The given half-wave potentials in the case of the reversible couple are equal to $E_{1/2} = (E_{pa} - E_{pc})/2$. Under brackets: ($\Delta E_p$, peak splitting in mV). [d] Not observed. ΔE_p is the difference potential between the oxidative and the reductive peak potentials. [e] Measured from DPV.

consequently the electron density would increase. The approach of the molecule with the side of the partially reduced trivanadate cap to exchange further electrons at the negatively polarized electrode thus becomes increasingly difficult because of the more important electrostatic repulsion.

Synthesis and characterization of the poly-ZnOEP–POM copolymers

Copolymer synthesis. We have shown that exhaustive electro-oxidation of zinc β-octaethylporphyrin (ZnOEP) in the presence of an excess of nucleophile at a potential of the first oxidation allows the formation of the mono-substituted zinc *meso*-Nu^+-β-octaethylporphyrin ($ZnOEP(Nu)^+$) in good yield.[48–50] This reactivity of oxidized porphyrins has been advantageously used to develop an easy and original method of electropolymerization of porphyrins when a difunctional nucleophile such as 4,4′-bipyridine was used.[51,52] When the iterative scans were performed at a sufficiently high potential in the anodic part (*i.e.* allowing the formation of the porphyrin dication), the formation of a conducting polymer with viologen spacers between porphyrins coating the working electrode was observed. Indeed, while the formation of radical cations was sufficient to perform mono-substitutions on porphyrins, the electropolymerization process required the formation of the dications, undoubtedly due to kinetic problems (the dications react faster with nucleophiles than the radical cations). Hence

an $E_1(E_{2i}C_{Nmeso}E_{2i+1}C_B)_{i=1\rightarrow n}E_{2(n+1)}$ mechanism can be proposed to explain the electropolymerization process where C_{Nmeso} corresponds to the nucleophilic attack at the *meso* position of the porphyrin which forms an isoporphyrin.[52,53]

The isoporphyrin is then oxidized (electrochemical step E_{2i+1}) and the proton present initially on the *meso*-carbon is released (chemical step C_B). For a degree of polymerization n, the corresponding global reaction can be written as:

$$(n+1)\text{ZnOEP} + (n+1)\text{Py-R-Py} \rightarrow \text{ZnOEP-(Py}^+\text{-R-Py}^+\text{-ZnOEP)}_n\text{-Py-R-Py} + (2n+1)\text{H}^+ + (4n+2)\text{e}^-(\text{R = spacer})$$

The reactions generated H^+ ions. According to previous work, scanning between −1.30 or −1.50 V and +1.80 V reduced these protons to H_2, and they were accumulated in solution when the scan was limited from 0.00 V to +1.80 V. Even in the second case, they did not perturb the coating of the electrodes. The demetalation of the metalloporphyrins was controlled by UV-visible spectroscopy and did not occur.

Thus, it is possible to easily modulate the nature of the bridging spacers between the porphyrin macrocycles. Indeed, instead of using 4,4′-bipyridine, this process of electropolymerization can be extended to molecules with various spacers between two pyridyl groups. The spacers can be selected for their specific chemical or structural properties: rigid or not; long or short; electron conducting or not; with conjugated π-bonds (alkene, alkyne or aromatic chains) or successive σ-bonds (alkyl chains), *etc.*, allowing one to modulate the communication between porphyrin macrocycles within the polymeric chains.

We applied this concept to POMs and prepared POM–porphyrin copolymer films with the Anderson type POM $[MnMo_6O_{18}\{(OCH_2)_3CNHCO(4\text{-}C_5H_4N)\}_2]^{3-}$ and ZnOEP,[40] which presented good photocatalytic[54,55] and photovoltaic[34] properties.

In the present work, all electropolymerizations have been carried out under the same experimental conditions by iterative scans in 0.1 mol L^{-1} solutions of tetrabutylammonium hexafluorophosphate in 1,2-$C_2H_4Cl_2$–CH_3CN (7 : 3) containing ZnOEP (0.25 mmol L^{-1}) and POM(py)$_2$ (0.25 mmol L^{-1}) under an argon atmosphere (Scheme 4).

Fig. 5 illustrates the evolution of the CVs during the electropolymerization of ZnOEP with **POM-dvb4,4**. Cyclic scanning was applied at potentials between −1.45 and 1.90 V *vs.* SCE or between −0.05 and +1.90 V *vs.* SCE. During the first scan in reduction, only signals assigned to the reduction of the **POM-dvb4,4** were detected between −0.05 and −1.45 V *vs.* SCE.

In the second scan, one additional irreversible reduction peak appeared between −0.75 to −0.95 V *vs.* SCE (peak a, Fig. 5), which corresponds to the reduction of the pyridinium units of the dipyridinium-POM spacers of the generated copolymer **poly-POM-dvb4,4-ZnOEP** (ZnOEP-Py$^+$-POM-Py$^+$)$_n$] (Scheme 3).[51,52,56–61] The height of this peak grew with repetitive scans at the beginning of the deposition and then reached a plateau. The irreversibility of the signal indicated that the generated pyridyl radicals are not stable and react further[62–64] as already observed in the case of copolymers with Anderson type POM.[40]

Similar behaviors were observed for the synthesis of copolymers **poly-POM-dvb3,4-ZnOEP**, **poly-POM-dvb4,4-ZnOEP** and **poly-POM-tvb3,3-ZnOEP** except that the reduction of the POM V^V/V^{IV} couple became more difficult to observe. Analogous electrochemical behavior was observed in the coordination complexes between $[MnMo_6O_{18}\{(OCH_2)_3CNHCO(4\text{-}C_5H_4N)\}_2]^{3-}$ and [Ru(CO)TPP] (TPP = tetraphenylporphyrin) or ZnTPP where it was noticed that the Mn^{III}/Mn^{II} redox process was remarkably slowed down with the quasi-complete disappearance of the electrochemical signal, even at the glassy carbon electrode.[13]

This significant electron-transfer rate constant attenuation is believed to be the consequence of long-distance electron transfer from the working electrode to the electroactive site of the molecule[65] because of the hindered approach of the POM to the electrode in the presence of coordinated porphyrin. A similar explanation can also be proposed in the present work where the coordination complex between ZnOEP and POM-(py)$_2$ can also be formed.

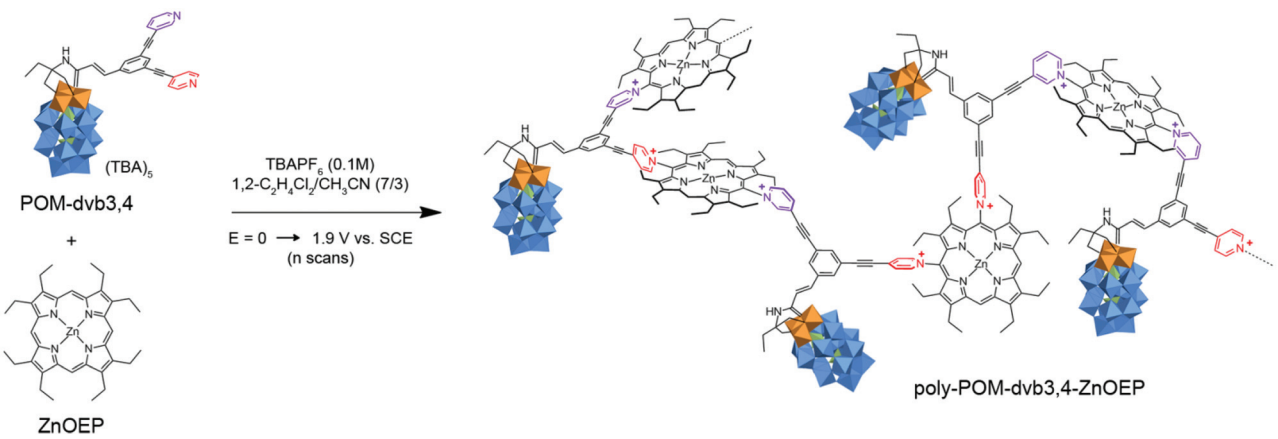

Scheme 4 Copolymer **poly-POM-dvb3,4-ZnOEP**, obtained with **POM-dvb3,4** and **ZnOEP**.

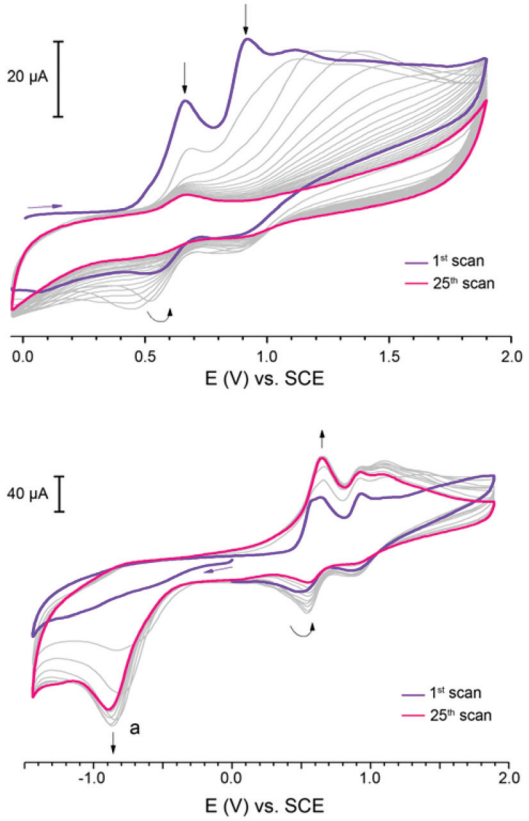

Fig. 5 Cyclic voltammograms for the electropolymerization of ZnOEP (0.25 mM) with **POM-dvb4,4** (0.25 mM) in 1,2-$C_2H_4Cl_2$–CH_3CN (7 : 3) $TBAPF_6$ 0.1 mol L^{-1}. Working electrode: ITO. S = 1 cm^2. Scan rate: 0.1 V s^{-1}. (←) Start of the scan. Cyclic scanning (0.1 V s^{-1}) was applied at potentials between −0.05 and +1.90 V *versus* SCE (top) and between −1.45 and 1.90 V *versus* SCE (bottom).

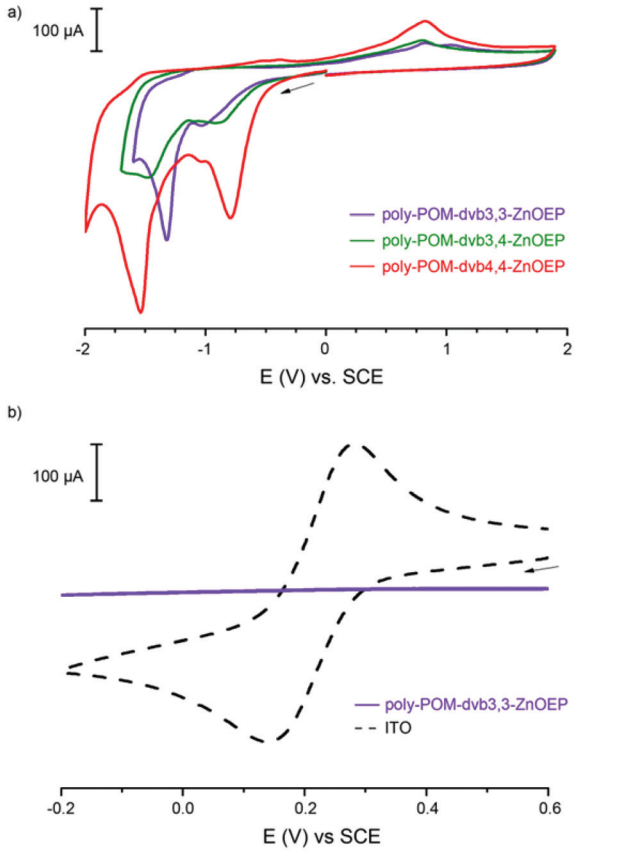

Fig. 6 (a) Cyclic voltammograms of **poly-POM-dvb3,3-ZnOEP**, **poly-POM-dvb3,4-ZnOEP** and **poly-POM-dvb4,4-ZnOEP** films (25 iterative scans between 0 and 1.90 V *versus* SCE) on ITO 1,2-$C_2H_4Cl_2$–CH_3CN (7 : 3) $(NBu_4)PF_6$ 0.1 mol L^{-1} at 100 mV s^{-1}. (b) Cyclic voltammograms of 1 mM of $K_3Fe(CN)_6$, in 0.5 M Na_2SO_4 of a modified ITO electrode with a poly-**POM-dvb3,3-ZnOEP** film (full violin line) and of a noncoated ITO electrode (dotted black line). v = 100 mV s^{-1}.

Cyclic voltammetry of the copolymeric films. The electrochemical behavior of these films has been studied by cyclic voltammetry (Fig. 6a). Typically, two irreversible reduction peaks appeared, which correspond to the pyridinium reductions and the first reduction of the ZnOEP macrocycle respectively (Table 2).

The pyridinium reductions were observed at −1.02 V, −0.87 V and −0.79 V *vs.* SCE for **poly-POM-dvb3,3-ZnOEP**, **poly-POM-dvb3,4-ZnOEP** and **poly-POM-dvb4,4-ZnOEP**, respectively, showing the strong influence of the isomer on the reduction potential of the pyridinium spacers. It can tentatively be explained in terms of π-conjugation (see ESI Fig. S4†). For **poly-POM-dvb4,4-ZnOEP**, the delocalization of the pyridyl radical is larger than for **poly-POM-dvb3,4-ZnOEP** because of the conjugation with the central benzene group, leading to a stabilisation of the reduced intermediate. In **poly-POM-dvb3,3-ZnOEP**, no stabilisation can occur since the delocalization of the radical is only possible within the pyridyl ring. The more stable reduced form was obtained at less negative potentials.

In contrast, the porphyrin reductions were measured at −1.32 V, −1.47 V and −1.57 V *vs.* SCE for **poly-POM-dvb3,3-ZnOEP**, **poly-POM-dvb3,4-ZnOEP** and **poly-POM-dvb4,4-ZnOEP**, respectively. These results show that when the delocalization of the radical of the reduced pyridinium is only possible onto the pyridyl ring, the localization of the radical is more on the nitrogen atom. It renders the reduction of the porphyrin easier because of the possibility of delocalization onto the macrocycle when the porphyrin is reduced. In the case of **poly-POM-dvb4,4-ZnOEP**, the reduction potential of the porphyrin is nearly the same as the potential measured for ZnOEP alone. Since the reduced pyridinium radical is delocalized on the entire **dvb4,4** ligand, delocalization of the reduced porphyrin radical is limited to the macrocycle. Thus, it explains a reduction potential of the ZnOEP subunit close to the potential measured for the starting ZnOEP.

The redox behavior of **poly-POM-tvb3,3-ZnOEP** is close to that of **poly-POM-dvb3,3-ZnOEP**, suggesting that conjugation to the POM is not crucial.

Permeability to anionic probes of the films. The permeability of these films toward electrochemically active probe molecules has also been studied. For a bare ITO electrode (unmodified), the redox probe $Fe(CN)_6^{3-}$ showed a quasi-reversible cyclic voltammetry (peak-to-peak separation 219 mV,

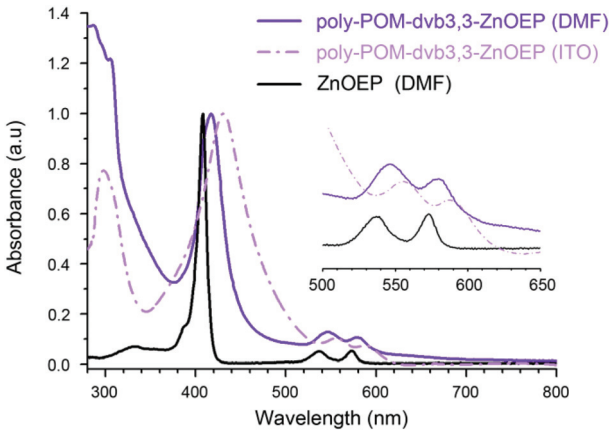

Fig. 7 Normalized UV-vis spectra of the modified ITO electrodes with **poly-POM-dvb3,3-ZnOEP** obtained after 25 iterative scans between 0 and 1.90 V *versus* SCE (dotted pink line), and of **poly-POM-dvb3,3-ZnOEP** (purple line) and of ZnOEP (black line) in DMF solution.

Fig. 6b, dotted-line), indicating that the probe diffuses freely to the ITO electrode surface and undergoes electron-transfer at the electrode. In contrast, in the presence of a **poly-POM-dvb3,3-ZnOEP** film, the peak current decreased a lot and reached zero. Similar behaviour was observed for **poly-POM-dvb3,4-ZnOEP** and **poly-POM-dvb4,4-ZnOEP**, but also for **poly-POM-tvb3,3-ZnOEP** films, suggesting that all these films were impermeable to $Fe(CN)_6^{3-}$.

UV-visible characterization of the copolymeric films. All the UV-visible spectra recorded on ITO electrodes coated with the copolymers presented identical characteristics. A typical UV-visible spectrum is represented in Fig. 7. The large Soret absorption band was red shifted compared to the ZnOEP monomer. This evolution can be understood by the exciton-coupling theory concerning intra- or intermolecular excitonic interactions between the ZnOEP subunits.[48,66–68] Similar spectral effects on dimeric or trimeric porphyrins have been reported and analyzed as dependent on the interporphyrin angles, the direction of the transition dipole moments in the monomer subunits, and also the distances between the porphyrins.[69–71]

The films were then removed from the ITO electrodes by dissolution in DMF. The profile of the UV-vis absorption bands of the solutions became sharper in comparison to those recorded on the solid films, but remained larger than for ZnOEP. This evolution suggests that for the most part intramolecular interactions remained when the copolymers were in solution.

X-ray photoelectron spectra (XPS)

This type of characterization has been employed to determine the elemental composition of the films. While XPS is not an accurate quantitative measurement of the individual atoms, it helps to determine the elements present and their oxidation states within the film. For example, the XPS measurement for **POM-dvb3,3-ZnOEP** (Fig. 8) confirms the presence of F, C, N, O, P, V and W for the copolymer onto the ITO electrode.

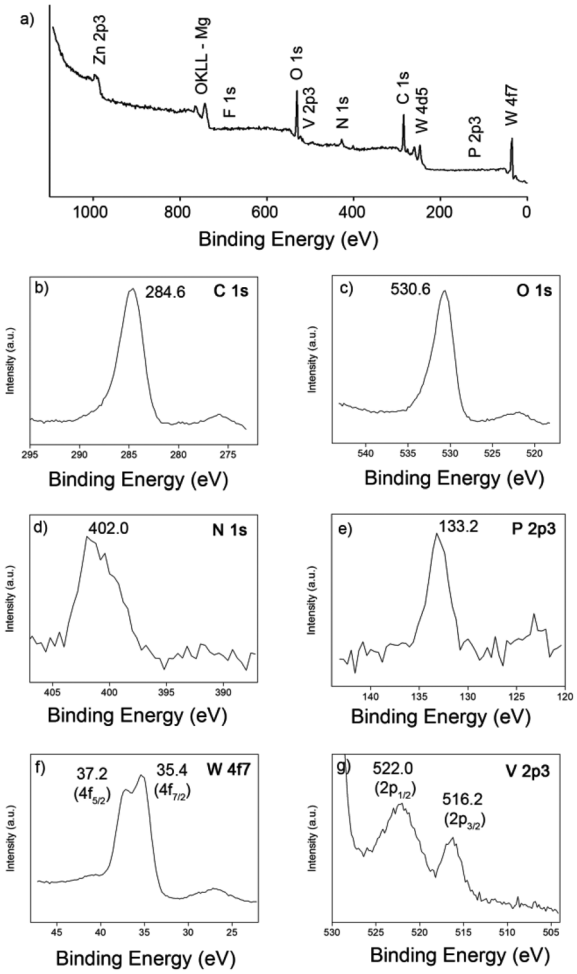

Fig. 8 XPS spectra of the modified ITO electrodes with **POM-dvb3,3-ZnOEP** obtained after 25 iterative scans between 0 and 1.90 V *versus* SCE. (a) Global XPS spectrum, (b) C1s, (c) O1s, (d) N1s, (e) P2p3, (f) W4f7, (g) V2p3.

The film exhibited peaks corresponding to P2p (133.2 eV), O1s (530.6 eV), V2p ($V2p_{1/2}$ = 522.0 eV and $V2p_{3/2}$ = 516.2 eV) and W4f levels ($W4f_{5/2}$ = 37.2 and $W4f_{7/2}$ = 35.4 eV) coming from the phosphorous, oxygen and tungsten atoms in the POM, while the C1s and N1s signals (at 284.6, 402.2 and 686.6 eV, respectively) result from the porphyrin ligand and the TBA counterions.

F1s signals (686.6 eV) can also be observed since PF_6^- anions can be trapped in the copolymer structure to balance pyridinium charge. Thus, both POM phosphates and PF_6^- contribute to the P2p peak. The signal of the Zn element is not detectable.

The XPS data confirm that we indeed incorporated the Dawson-type phosphovanadotungstate and the zinc metalloporphyrin into the films, which is in agreement with the UV-vis absorption results. Similar XPS spectra (see ESI Fig. S7†) have been obtained for **poly-POM-dvb3,4-ZnOEP** and **poly-POM-dvb4,4-ZnOEP**.

Copolymer morphology (atomic force microscopy). The coated electrodes were washed with CH_2Cl_2 to remove any trace of the conducting salt present on the film and were

examined by scanning atomic force microscopy (AFM). Copolymer **poly-POM-dvb3,3-ZnOEP** appeared in the form of tightly packed coils as already observed in the case of the copolymer with an Anderson type polyanion. The morphology did not depend on whether the coated electrodes were obtained by scanning over the potential ranging from −1.30 to +1.90 V (Fig. 9b) or only from −0.05 to +1.90 V *vs.* SCE.

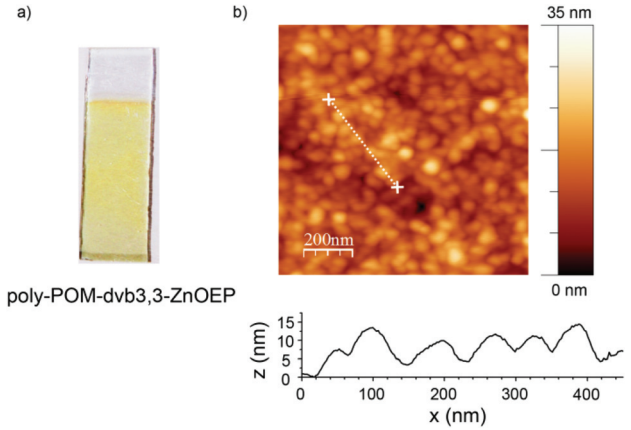

Fig. 9 (a) Picture of the ITO modified electrode with a **poly-POM-dvb3,3-ZnOEP** copolymer obtained after 25 iterative scans between 0 and 1.90 V *versus* SCE. (b) Tapping mode AFM topography of the film on ITO. Bottom: section analysis of the marked white dotted line on the image.

The rms surface roughness of the film obtained by 25 iterative scans from −0.05 to +1.90 V *vs.* SCE was 6.32 nm for a 1 μm^2 area. The AFM studies showed an increase in the rms surface roughness with the number of iterative scans.

Similar results have been obtained for **poly-POM-dvb3,4-ZnOEP** (rms surface roughness: 5.53 nm), **poly-POM-dvb4,4-ZnOEP** (rms surface roughness: 4.21 nm) and **poly-POM-tvb3,3-ZnOEP** (rms surface roughness: 3.20 nm).

Control of the thickness of copolymeric films. We have also examined the control of the thickness of the deposited polymeric film. For that, two ways of preparation of the polymer coated onto the ITO electrode have been followed. In the first experiment, coated electrodes were prepared just by changing the number of iterative scans n during the electropolymerization. A plot of the absorbance at λ = 427 nm (Soret band of the porphyrin) as a function of the number of scans n (Fig. 10a

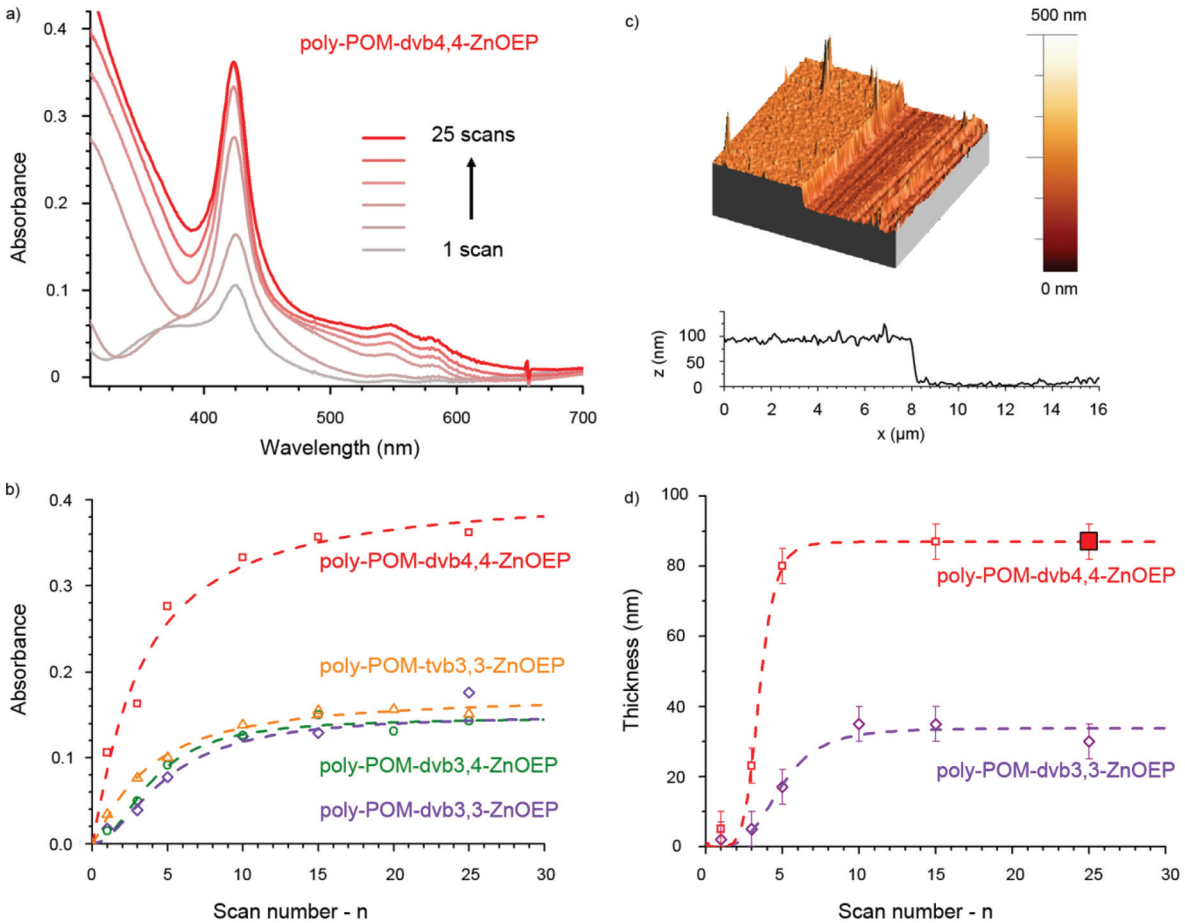

Fig. 10 (a) UV-visible absorption spectra of **poly-POM-dvb4,4-ZnOEP** (onto ITO) with different numbers of iterative scans (between 0 and +1.90 V *versus* SCE). Only one side is recovered by ITO. (b) Plots of the absorbance, measured at λ = 427 nm, *versus* the numbers of iterative scans for **poly-POM-dvb3,3-ZnOEP**, **poly-POM-dvb3,4-ZnOEP**, **poly-POM-dvb4,4-ZnOEP**, and **poly-POM-tvb3,3-ZnOEP**. (c) Atomic force micrograph (AFM, surface plot) image of the modified ITO electrode with **poly-POM-dvb4,4-ZnOEP** obtained after 25 iterative scans. Bottom: section analysis. (d) Thickness measured from AFM *versus* different numbers of iterative scans (between −0.05 and 1.90 V *vs.* SCE). The red filled black square corresponds to the measurement obtained from (c).

and 10b) shows effectively an increase of the thickness during the first scans and then a constant value. In the second experiment, the thicknesses of the films measured by AFM confirmed this point (Fig. 10c and 10d).

To measure the thickness, we removed the polymer by scratching the film with a metallic tip, and clearly observed some puffiness induced by the material removal. Analysis of the bottom indicated that we reached the ITO substrate. The thickness was estimated by comparing the height on each side, far from the puffiness. Interestingly, the estimated thickness increased with the scan number with nearly the same trend as the UV-Vis absorbance intensity.

Such behavior fits with the decrease of the film conductivity already observed during the electropolymerization (Fig. 5). Thus, the deposition which is initially very efficient becomes gradually more difficult and eventually stops. In addition, in the case of **poly-POM-dvb4,4-ZnOEP**, with the same number of iterative scans, the thickness is nearly three times more important. This result can be explained by the better conductivity of the films when using the fully conjugated **dvb4,4** ligand.

Conclusion

In the present paper we have prepared four films from the anodic electro-copolymerization of organo-POM bricks with designed geometries and structures, and a porphyrin. The bricks as well as the materials were unambiguously characterized by several analytical techniques.

The conclusion of the aggregated characterizations shows that the conjugation to the POM may not be a crucial item, at least from an electrochemical point of view, but the geometry of the pyridines on the hybrid monomer is directly related to the performances of the materials.

Future work will focus on the assessment of the reactivity of the materials under visible light irradiation.

Acknowledgements

We thank CNRS, Université Paris-Sud (Orsay, France), the University of Strasbourg (France), Université Paris-Descartes (Paris, France), Université Pierre et Marie Curie (Paris, France), ECE Paris Ecole d'Ingénieurs (France), IDEX Attractivité 2012 and Fudan University (Shanghai, China) for funding of this work. We also thank the Délégation Générale à l'Armement (DGA) for a Ph.D. fellowship.

Notes and references

1 D.-L. Long, R. Tsunashima and L. Cronin, *Angew. Chem., Int. Ed.*, 2010, **49**, 1736–1758.
2 C. Streb, *Dalton Trans.*, 2012, **41**, 1651–1659.
3 L. Ruhlmann, C. Costa-Coquelard, J. Hao, S. Jiang, C. He, L. Sun and I. Lampre, *Can. J. Chem.*, 2008, **86**, 1034–1043.
4 J. Ettedgui, Y. Diskin-Posner, L. Weiner and R. Neumann, *J. Am. Chem. Soc.*, 2011, **133**, 188–190.
5 J. J. Walsh, D.-L. Long, L. Cronin, A. M. Bond, R. J. Forster and T. E. Keyes, *Dalton Trans.*, 2011, **40**, 2038–2045.
6 J. Xie, B. F. Abrahams and A. G. Wedd, *Chem. Commun.*, 2008, 576–578.
7 S. Nie, Y. Zhang, B. Liu, Z. Li, H. Hu, G. Xue, F. Fu and J. Wang, *J. Solid State Chem.*, 2010, **183**, 2957–2962.
8 H. Zhang, J. Peng, Y. Shen, X. Yu, F. Zhang, J. Mei, B. Li and L. Zhang, *Chem. Commun.*, 2012, **48**, 4462–4464.
9 A. Tsuda, E. Hirahara, Y.-S. Kim, H. Tanaka, T. Kawai and T. Aida, *Angew. Chem., Int. Ed.*, 2004, **43**, 6327–6331.
10 I. C. M. S. Santos, S. L. H. Rebelo, M. S. S. Balula, R. R. L. Martins, M. M. M. S. Pereira, M. M. Q. Simões, M. G. P. M. S. Neves, J. a. S. Cavaleiro and A. M. V. Cavaleiro, *J. Mol. Catal. A: Chem.*, 2005, **231**, 35–45.
11 C. Costa-Coquelard, S. Sorgues and L. Ruhlmann, *J. Phys. Chem. A*, 2010, **114**, 6394–6400.
12 A. Yokoyama, T. Kojima, K. Ohkubo, M. Shiro and S. Fukuzumi, *J. Phys. Chem. A*, 2011, **115**, 986–997.
13 C. Allain, S. Favette, L. Chamoreau, J. Vaissermann, L. Ruhlmann and B. Hasenknopf, *Eur. J. Inorg. Chem.*, 2008, **2008**, 3433–3441.
14 A. Falber, B. P. Burton-Pye, I. Radivojevic, L. Todaro, R. Saleh, L. Francesconi and C. M. Drain, *Eur. J. Inorg. Chem.*, 2009, 2459–2466.
15 D. Schaming, C. Costa-Coquelard, I. Lampre, S. Sorgues, M. Erard, X. Liu, J. Liu, L. Sun, J. Canny, R. Thouvenot and L. Ruhlmann, *Inorg. Chim. Acta*, 2010, **363**, 2185–2192.
16 A. Dolbecq, E. Dumas, C. R. Mayer and P. Mialane, *Chem. Rev.*, 2010, **110**, 6009–6048.
17 A. Proust, B. Matt, R. Villanneau, G. Guillemot, P. Gouzerh and G. Izzet, *Chem. Soc. Rev.*, 2012, **41**, 7605–7622.
18 J. L. Stark, V. G. Young and E. A. Maatta, *Angew. Chem., Int. Ed.*, 1995, **34**, 2547–2548.
19 J. Kang, J. A. Nelson, M. Lu, B. Xie, Z. Peng and D. R. Powell, *Inorg. Chem.*, 2004, **43**, 6408–6413.
20 F. Odobel, M. Séverac, Y. Pellegrin, E. Blart, C. Fosse, C. Cannizzo, C. R. Mayer, K. J. Elliott and A. Harriman, *Chem.–Eur. J*, 2009, **15**, 3130–3138.
21 B. Matt, C. Coudret, C. Viala, D. Jouvenot, F. Loiseau, G. Izzet and A. Proust, *Inorg. Chem.*, 2011, **50**, 7761–7768.
22 J. Gao, X. Liu, Y. Liu, L. Yu, Y. Feng, H. Chen, Y. Li, G. Rakesh, C. H. A. Huan, T. C. Sum, Y. Zhao and Q. Zhang, *Dalton Trans.*, 2012, **41**, 12185–12191.
23 B. Matt, J. Moussa, L.-M. Chamoreau, C. Afonso, A. Proust, H. Amouri and G. Izzet, *Organometallics*, 2012, **31**, 35–38.
24 K. J. Elliott, A. Harriman, L. Le Pleux, Y. Pellegrin, E. Blart, C. R. Mayer and F. Odobel, *Phys. Chem. Chem. Phys.*, 2009, **11**, 8767–8773.
25 M. Araghi, V. Mirkhani, M. Moghadam, S. Tangestaninejad and I. Mohammdpoor-Baltork, *Dalton Trans.*, 2012, **41**, 3087–3094.
26 M. Araghi, V. Mirkhani, M. Moghadam, S. Tangestaninejad and I. Mohammdpoor-Baltork, *Dalton Trans.*, 2012, **41**, 11745–11752.

27 (*a*) C. Allain, D. Schaming, N. Karakostas, M. Erard, J.-P. Gisselbrecht, S. Sorgues, I. Lampre, L. Ruhlmann and B. Hasenknopf, *Dalton Trans.*, 2013, **42**, 2745–2754. For an alternative approach and potential use of POM–porphyrin materials, see: (*b*) D. Hagrman, P. J. Hagrman and J. Zubieta, *Angew. Chem., Int. Ed.*, 1999, **38**, 3165–3168.
28 S. Liu and Z. Tang, *Nano Today*, 2010, **5**, 267–281.
29 J. Zhu, Q. Zeng, S. O'Carroll, A. Bond, T. E. Keyes and R. J. Forster, *Electrochem. Commun.*, 2011, **13**, 899–902.
30 J. J. Walsh, C. T. Mallon, A. M. Bond, T. E. Keyes and R. J. Forster, *Chem. Commun.*, 2012, **48**, 3593–3595.
31 Y. Wang and C. Hu, *Thin Solid Films*, 2005, **476**, 84–91.
32 S. Gao, R. Cao and C. Yang, *J. Colloid Interface Sci.*, 2008, **324**, 156–166.
33 G. Bazzan, W. Smith, L. C. Francesconi and C. M. Drain, *Langmuir*, 2008, **24**, 3244–3249.
34 I. Ahmed, R. Farha, M. Goldmann and L. Ruhlmann, *Chem. Commun.*, 2013, **49**, 496–498.
35 J. Kang, B. Xu, Z. Peng, X. Zhu, Y. Wei and D. R. Powell, *Angew. Chem., Int. Ed.*, 2005, **44**, 6902–6905.
36 L. Xu, M. Lu, B. Xu, Y. Wei, Z. Peng and D. R. Powell, *Angew. Chem., Int. Ed.*, 2002, **41**, 4129–4132.
37 M. Lu, B. Xie, J. Kang, F. C. Chen, Y. Yang and Z. Peng, *Chem. Mater.*, 2005, **17**, 402–408.
38 S. Chakraborty, A. Keightley, V. Dusevich, Y. Wang and Z. Peng, *Chem. Mater.*, 2010, **22**, 3995–4006.
39 B. Xu, M. Lu, J. Kang, D. Wang, J. Brown and Z. Peng, *Chem. Mater.*, 2005, **17**, 2841–2851.
40 D. Schaming, C. Allain, R. Farha, M. Goldmann, S. Lobstein, A. Giraudeau, B. Hasenknopf and L. Ruhlmann, *Langmuir*, 2010, **26**, 5101–5109.
41 J. Li, I. Huth, L.-M. Chamoreau, B. Hasenknopf, E. Lacôte, S. Thorimbert and M. Malacria, *Angew. Chem., Int. Ed.*, 2009, **48**, 2035–2038.
42 Y. Hou and C. L. Hill, *J. Am. Chem. Soc.*, 1993, **115**, 11823–11830.
43 S. K. Deb, T. M. Maddux and L. Yu, *J. Am. Chem. Soc.*, 1997, **119**, 9079–9080.
44 S. M. Courtney, P. A. Hay and D. I. C. Scopes, *WO* 2004/046122 A2, 2004.
45 C. Desmarets, I. Azcarate, G. Gontard and H. Amouri, *Eur. J. Inorg. Chem*, 2011, 4558–4563.
46 R. G. Finke, B. Rapko, R. J. Saxton and P. J. Domaille, *J. Am. Chem. Soc.*, 1986, **108**, 2947–2960.
47 R. G. Finke, M. W. Droege and P. J. Domaille, *Inorg. Chem.*, 1987, **26**, 3886–3896.
48 A. Giraudeau, L. Ruhlmann, L. El Kahef and M. Gross, *J. Am. Chem. Soc.*, 1996, **118**, 2969–2979.
49 L. Ruhlmann and A. Giraudeau, *Chem. Commun.*, 1996, 2007–2008.
50 L. Ruhlmann and A. Giraudeau, *Eur. J. Inorg. Chem.*, 2001, **2001**, 659–668.
51 L. Ruhlmann, A. Schulz, A. Giraudeau, C. Messerschmidt and J.-H. Fuhrhop, *J. Am. Chem. Soc.*, 1999, **121**, 6664–6667.
52 L. Ruhlmann, J. Hao, Z. Ping and A. Giraudeau, *J. Electroanal. Chem.*, 2008, **621**, 22–30.
53 D. Schaming, I. Ahmed, J. Hao, V. Alain-Rizzo, R. Farha, M. Goldmann, H. Xu, A. Giraudeau, P. Audebert and L. Ruhlmann, *Electrochim. Acta*, 2011, **56**, 10454–10463.
54 D. Schaming, C. Costa-Coquelard, S. Sorgues, L. Ruhlmann and I. Lampre, *Appl. Catal., A: Gen.*, 2010, **373**, 160–167.
55 D. Schaming, R. Farha, H. Xu, M. Goldmann and L. Ruhlmann, *Langmuir*, 2011, **27**, 132–143.
56 A. Giraudeau, D. Schaming, J. Hao, R. Farha, M. Goldmann and L. Ruhlmann, *J. Electroanal. Chem.*, 2010, **638**, 70–75.
57 J. Hao, A. Giraudeau, Z. Ping and L. Ruhlmann, *Langmuir*, 2008, **24**, 1600–1603.
58 M. A. Oturan, P. Dostert, M. S. Benedtti, J. Moiroux, A. Anne and M. B. Fleury, *J. Electroanal. Chem.*, 1988, **242**, 171–179.
59 V. Carelli, F. Liberatore, A. Casini, S. Tortorella, L. Scipione and B. Di Rienzo, *New J. Chem.*, 1998, **22**, 999–1004.
60 J. E. H. Buston, H. L. Anderson and F. Marken, *Chem. Commun.*, 2001, 1046–1047.
61 V. Carelli, F. Liberatore, S. Tortorella, B. Di Rienzo and L. Scipione, *J. Chem. Soc., Perkin Trans. 1*, 2002, 542–547.
62 A. Brisach-Wittmeyer, S. Lobstein, M. Gross and A. Giraudeau, *J. Electroanal. Chem.*, 2005, **576**, 129–137.
63 A. Giraudeau, H. J. Callot and M. Gross, *Inorg. Chem.*, 1979, **18**, 201–206.
64 D. Schaming, A. Giraudeau, S. Lobstein, R. Farha, M. Goldmann, J.-P. Gisselbrecht and L. Ruhlmann, *J. Electroanal. Chem.*, 2009, **635**, 20–28.
65 P. J. Dandliker, F. Diederich, A. Zingg, J. Gisselbrecht, M. Gross, A. Louati and E. Sanford, *Helv. Chim. Acta*, 1997, **80**, 1773–1801.
66 M. Kasha, *Rev. Mod. Phys.*, 1959, **31**, 162–169.
67 J. L. Sessler, M. R. Johnson, S. E. Creager, J. C. Fettinger and J. a. Ibers, *J. Am. Chem. Soc.*, 1990, **112**, 9310–9329.
68 L. Ruhlmann, M. Gross and A. Giraudeau, *Chem.–Eur. J.*, 2003, **9**, 5085–5096.
69 I. Tabushi, S. Kugimiya, M. G. Kinnaird and T. Sasaki, *J. Am. Chem. Soc.*, 1985, **107**, 4192–4199.
70 J. L. Sessler, J. Hugdahl and M. R. Johnson, *J. Org. Chem.*, 1986, **51**, 2838–2840.
71 Y. Won, R. A. Friesner, M. R. Johnson and J. L. Sessler, *Photosynth. Res.*, 1989, **22**, 201–210.

